Modeling and sensitivity analysis of consensus algorithm based distributed hierarchical control for dc microgrids

Meng, Lexuan; Dragicevic, Tomislav; Vasquez, Juan Carlos; Guerrero, Josep M.; Roldan Perez, Javier

Published in:
Proceedings of the 2015 IEEE Applied Power Electronics Conference and Exposition (APEC)

DOI (link to publication from Publisher):
10.1109/APEC.2015.7104373

Publication date:
2015

Document Version
Early version, also known as pre-print

Modeling and Sensitivity Analysis of Consensus Algorithm Based Distributed Hierarchical Control for DC Microgrids

Lexuan Meng, Tomislav Dragicevic, Juan C. Vasquez, Josep M. Guerrero
Denmark Microgrids Research Programme: www.microgrids.et.aau.dk
Department of Energy Technology
Aalborg University,
Aalborg, Denmark
{lme, tdr, juq, joz}@et.aau.dk

Javier Roldán Pérez
School of Engineering
Comillas Pontifical University,
Madrid, Spain
Javier.Roldan@iit.upcomillas.es

***Abstract*— Distributed control methods for microgrid systems become a popular topic in recent years. Distributed algorithms, such as consensus algorithms, can be applied for distributed information sharing. However, by using this kind of algorithms the stability analysis becomes a critical issue since the dynamics of electrical and communication systems interact with each other. Apart from that, the communication characteristics also affect the dynamics of the system. Due to discrete nature of information exchange in communication network, Laplace domain analysis is not accurate enough for this kind of dynamic study. The aim of this paper is to model the complete DC microgrid system in z-domain and perform sensitivity analysis for the complete system. A generalized modeling method is proposed and the system dynamics under different control parameters, communication topologies and communication speed are studied. The responses derived from the analytical model are verified by comparing them with Simulink/PLECS based simulation results.**

Keywords—DC microgrids, DC/DC converters, consensus algorithm, distributed hierarchical control, discrete-time modeling

I. INTRODUCTION

Microgrid (MG) concept was proposed for efficient use and integration of distributed resources (DR), storage systems, and consumers [1]. It can operate in either islanded or grid-connected modes, tending to increase the flexibility and security of energy system by being able to switch seamlessly between them. A number of methods have been proposed to achieve different MG control objectives [2]–[4], such as appropriate power sharing, enhanced power quality, optimized energy efficiency, DR coordination, and so on.

Hierarchical control [2], [3] is generally applied for MG system to simultaneously realize control objectives in different technical areas and time scales, as shown in Fig. 1. Primary control is in charge of proper power sharing among DRs. Local droop control is usually used in primary level in each controller, as it is accepted as a reasonable way to achieve communication-less distributed power sharing control.

Secondary control can help to keep the desirable power quality within the system and provide ancillary services. Based on this hierarchy, the way of implementing the control can be centralized or distributed. For example, in order to recover the

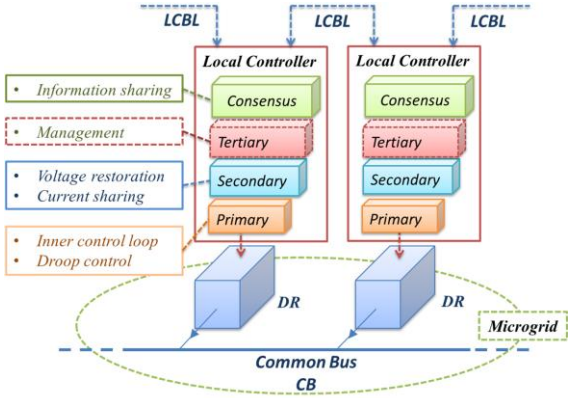

Fig. 1. Distributed hierarchical control for microgrids.

voltage and frequency deviation caused by droop control, centralized and distributed secondary control for voltage and frequency restoration are presented in [2] and [6] respectively. A distributed cooperative control for DC microgrids is proposed in [7] achieving both bus voltage correction and accurate current sharing. In the top level, tertiary control can be also implemented for the purpose of energy management and optimization of economic issues. A system efficiency optimization method is proposed in [8]. Here, a genetic algorithm is implemented in tertiary control's central controller to minimize the losses of the whole system. On the other side, attempts have been made to achieve distributed management. For that matter, consensus algorithm is often used. A distributed decision-making based on a dynamic consensus algorithm (DCA) was implemented in [13] for automatic load restoration. A consensus theory based distributed coordination scheme for microgrid via wireless communication is proposed in [14] to coordinate the generation, storage and consumption.

For both secondary and tertiary control, low bandwidth communication links (LBCL) are commonly used for data transmission [16], as shown in Fig. 1. In general, when considering the initial investment in the communication network, as well as flexibility and reliability of the system, distributed control methods are usually preferred.

However, although allegedly superior in many ways, modeling and stability analysis for these kinds of control

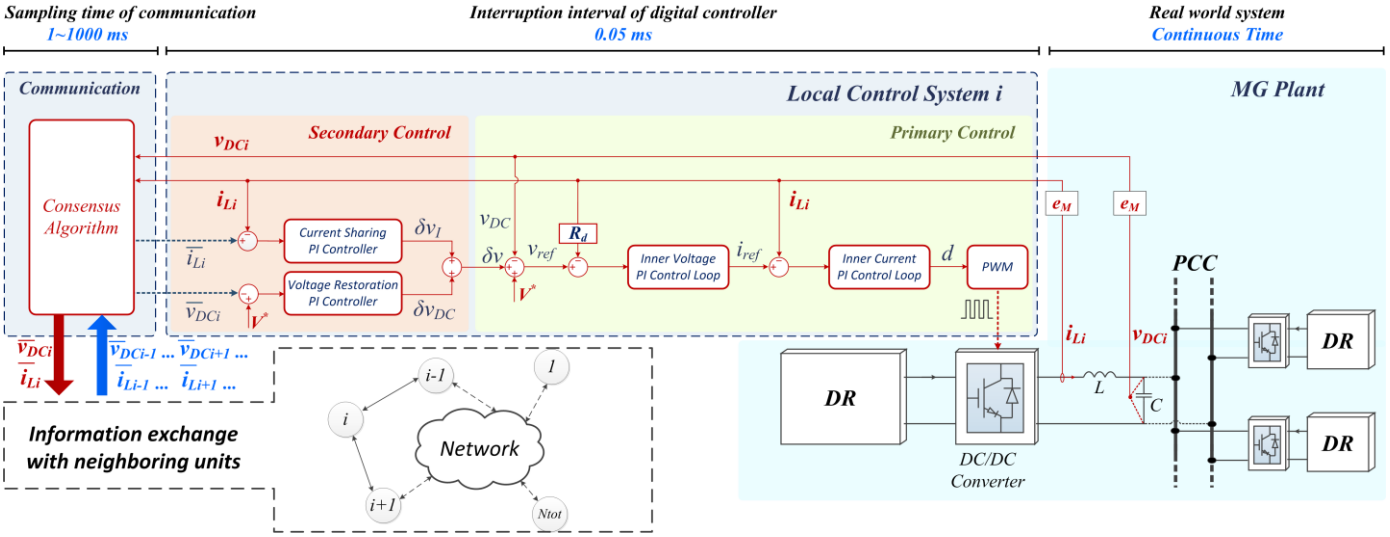

Fig. 2. Distributed hierarchical control for DC microgrids.

systems in practical applications are rarely studied. In particular, the inclusion of consensus algorithm in the finite-speed-communication links becomes a challenge when paired with dynamics of electrical network. Laplace-domain (s) continuous-time (CT) model is then not accurate enough to represent the overall system behavior, due to different nature of electrical, digital control and communication part. In that sense, the electrical part, which includes the filter, transmission lines and loads, is actually a CT system, while the digital controller and communication network are discrete-time (DT) systems. Moreover, sampling times of control and communication significantly differ with typical times for the matter being in μs range and ms range respectively. In order to analyze this kind of system, z-domain DT modeling is applied in this paper taking into account the discrete nature of measurement sampling, controller implementation and communication.

A DC microgrid with primary and secondary control is taken as the study case. The paper is organized as follows. Section II introduces the principles of distributed hierarchical control for DC microgrids. The basics of consensus algorithm are presented in Section III. Section IV proposes the modeling method, based on which the system state space (SS) model is established. Section V shows the comparison of the SS model with Simulink/PLECS (SP) simulation results, and the sensitivity of overall system is studied. Section VI gives the conclusion.

II. Distributed Hierarchical Control Scheme

A consensus algorithm based distributed hierarchical control scheme for a DC microgrid is shown in Fig. 2. The distributed generator is considered as a DR connected through an interfacing DC/DC converter with associated LC filter that is connected to the common bus (CB) as well as the loads.

The local control system includes primary control loops and secondary control loops. Primary control is in charge of voltage and current regulation. Proportional integral (PI) controllers are used in inner voltage and current control loops:

$$d = (\frac{K_{ic}}{s} + K_{pc}) \cdot (i_{ref} - i_{Li}) \tag{1}$$

$$i_{ref} = (\frac{K_{iv}}{s} + K_{pv}) \cdot (V^* + \delta v - v_{DC} - i_{Li} R_d) \tag{2}$$

where s is the *Laplace* operator, d is the duty ratio for pulse width modulation (PWM), i_{ref} is the current reference, V^* is the voltage reference, δv is the compensating voltage term generated by secondary control, v_{DC} and i_{Li} are the measured CB voltage and output current, K_{ic} and K_{pc} are the integral and proportional term of current PI controller, K_{iv} and K_{pv} are the integral and proportional term of voltage PI controller. A virtual resistance R_d feedback (often referred to as the droop control [2], [3]) is also implemented for better current sharing and system damping.

However, voltage deviation inevitably appears when droop control is applied. Also, the load current cannot be accurately shared when distribution lines are different in parameters or measurement errors are considered. Secondary control can be installed to avoid these problems:

$$\delta v_I = (\frac{K_{isc}}{s} + K_{psc}) \cdot (\overline{i_L} - i_{Li}) \tag{3}$$

$$\delta v_{DC} = (\frac{K_{isv}}{s} + K_{psv}) \cdot (\overline{v_{DC}} - V^*) \tag{4}$$

where δv_I and δv_{DC} are the compensating terms for current sharing and voltage restoration, respectively. $\overline{i_L}$ and $\overline{v_{DC}}$ are the averaged output current and CB voltage of all the DR units, K_{isc} and K_{psc} are the integral and proportional term of current sharing controller, K_{isv} and K_{psv} are the integral and proportional term of voltage restoration controller. The summation of δv_I and δv_{DC} is sent to primary controller.

On the top of the controller, consensus algorithm is implemented for information sharing among a set of distributed agents. It helps to discover the averaged value of total generation current $\overline{i_L}$ and measured CB voltage $\overline{v_{DC}}$. The details are introduced in the following Section.

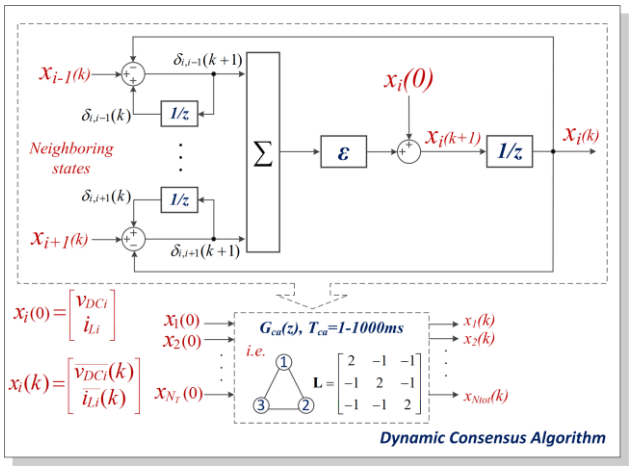

Fig. 3. Dynamic consensus algorithm model

III. Dynamic Consensus Algorithm

The general purpose of consensus algorithm is to allow a set of distributed agents to reach an agreement on a quantity of interest by exchanging information through communication network. In case of MG systems, these algorithms can achieve the information sharing and coordination among distributed generators, consumers and storage systems. *Graph Laplacians* [19] describe the underlying communication structure in these kinds of systems and play a pivotal role in their convergence and dynamic analysis.

A. Dynamic Consensus Algorithm

Considering the discrete nature of communication data transmission, DT form of the consensus algorithm is considered in this paper, which can be described as [17], [18]:

$$x_i(k+1) = x_i(k) + \varepsilon \cdot \sum_{j \in N_i} a_{ij} \cdot (x_j(k) - x_i(k)) \tag{5}$$

where i=1,2,…,N_T, N_T is the total number of agent nodes. x_i is the state of agent i. a_{ij} indicates the connection status between node i and node j, a_{ij}=0 if the nodes i and j are not linked. N_i is the set of indexes of the agents that can be connected with agent i, and ε is the constant edge weight used for tuning the dynamic of DCA. In addition, in order to ensure the accurate consensus in dynamically changing environment, a modified version of the algorithm, referred to as dynamic consensus algorithm (DCA) [20], is applied in this paper (see Fig. 3):

$$x_i(k+1) = x_i(0) + \varepsilon \cdot \sum_{j \in N_i} \delta_{ij}(k+1) \tag{6}$$

$$\delta_{ij}(k+1) = \delta_{ij}(k) + a_{ij} \cdot \left(x_j(k) - x_i(k)\right) \tag{7}$$

where $\delta_{ij}(k)$ stores the cumulative difference between two agents, and $\delta_{ij}(0) = 0$. Based on (6) and (7), it is explicit that the final consensus value depends on initial value $x_i(0)$, and regardless of any changes to $x_i(0)$, the algorithm will converge to an appropriate average value.

From the system point of view, vector form of the iteration algorithm can be expressed as [17], [18]:

$$\mathbf{x}(k+1) = \mathbf{W} \cdot \mathbf{x}(k) \tag{8}$$

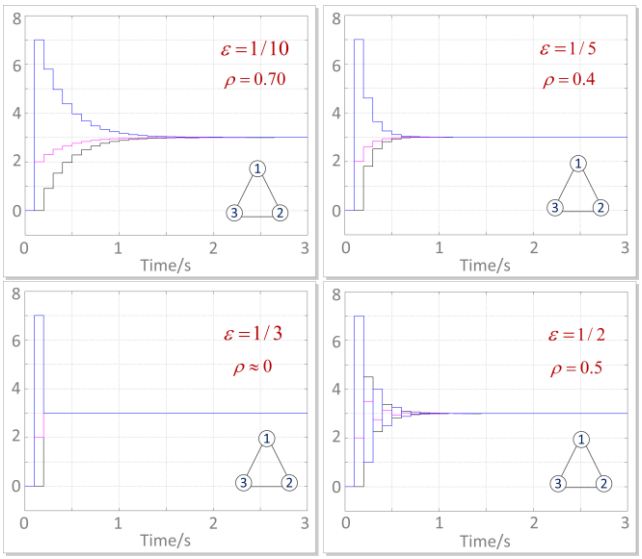

Fig. 4. DCA dynamics under different constant edge weight

where $\mathbf{x}$ is the state vector $\mathbf{x}(k) = [x_1(k), x_2(k), ..., x_{N_T}(k)]^T$, $\mathbf{W}$ is the *weight matrix* of the communication network, if constant edge weight ε is considered, $\mathbf{W}$ can be described as:

$$\mathbf{W} = \mathbf{I} - \varepsilon \cdot \mathbf{L} \tag{9}$$

where $\mathbf{L}$ is the laplacian matrix of the communication network (see Fig. 3) [21], [22], N_i is the set of indexes of the agents that are connected with agent i, N_T is the total number of agents. The final consensus equilibrium $\mathbf{x}_{eq}$ is:

$$\mathbf{x}_{eq} = \lim_{k \to \infty} \mathbf{x}(k) = \lim_{k \to \infty} \mathbf{W}^k \mathbf{x}(0) = \left(\frac{1}{N_T} \mathbf{1} \cdot \mathbf{1}^T \right) \mathbf{x}(0) \tag{10}$$

where $\mathbf{x}(0) = [\mathbf{x}_1(0), \mathbf{x}_2(0), ..., \mathbf{x}_{N_T}(0)]$ is the vector of the initial values held by each agent, $\mathbf{1}$ denotes the vector with all the elements 1. The detailed proof of the convergence can be found in [18]. In this paper, the initial values are the locally measured CB voltage (v_{DCi}) and inductor current (i_{Li}).

B. DCA Convergence and Dynamics

In order to ensure the stability and fast convergence of the communication algorithm, ε has to be properly chosen. As bidirectional communication links are considered, the problem of finding the fastest rate is referred to as the symmetric fastest distributed linear averaging (*symmetric FDLA*) problem. It is actually the minimization of spectral radius (ρ) of the matrix $\mathbf{W} - (1/N_T) \cdot \mathbf{1} \cdot \mathbf{1}^T$ with certain constraints on *weight* matrix $\mathbf{W}$. The fastest convergence is ensured when [23]:

$$\varepsilon = \frac{2}{\lambda_1(L) + \lambda_{n-1}(L)} \tag{11}$$

where $\lambda_j(\cdot)$ denotes the j^{th} largest eigenvalue of a symmetric matrix. Based on the topology of Fig. 3, the eigenvalues of $\mathbf{L}$ are $[0\ 3\ 3]^T$ which gives the optimal ε=1/3. The convergence speed is compared in Fig. 4 as an example. In this case, the sampling time of the consensus algorithm is set to T_{ca}=100ms. The system starts with $\mathbf{x}(0) = [0, 2, 7]$ and converges to average value 3. According to the results in Fig. 4, the constant edge weight ε has pivotal influence over the dynamic of the DCA, and when ε=1/3 the system has minimized spectral radius $\rho(\mathbf{W} - (1/N_T) \cdot \mathbf{1} \cdot \mathbf{1}^T)$ and fastest converging speed.

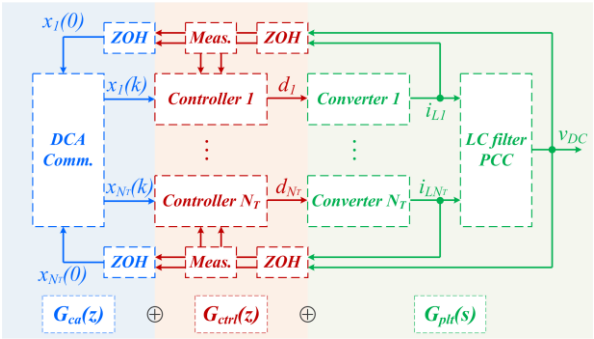

Fig. 5. Structure of complete system model.

IV. System Modeling

Considering the different features and sampling times, the system is modeled with three parts separately, as shown in Fig. 5: 1) microgrid plant model $\boldsymbol{G_{plt}}(s)$ (DR, converter, filter and load), 2) controller model $\boldsymbol{G_{ctrl}}(s)$ (primary control and secondary control), 3) communication part model $\boldsymbol{G_{ca}}(s)$ (consensus algorithm, communication topology).

A. MG Plant

The DC MG plant model is shown in Fig. 6. DR is simplified as a DC source, which is connected to CB through a DC/DC converter and LC filter. Buck converters are used in this particular study case. They convert input voltage v_{in} to output voltage v_o that appears at the common DC bus. Resistive loads (R_{load}) that are also connected to CB are considered in this paper. Averaged model of the DC/DC converter is used. If a total number of N_T DRs and converters are connected in parallel, the plant model can be described as:

$$i_{Li} = \frac{v_{in}}{sL}\cdot d - \frac{1}{sL}\cdot v_{DC} \tag{12}$$

$$v_{DC} = \frac{\sum i_{Li}}{N_T \cdot sC} - \frac{v_{DC}}{N_T R_{load}\cdot sC} \tag{13}$$

A transfer function $G_{plt}(s)$ can be obtained with duty ratios $[d_1, d_2, \ldots, d_{NT}]$ as inputs, inductor current $[i_{L1}, i_{L2}, \ldots, i_{LNT}]$ and CB voltage v_{DC} as outputs. The SS model of the MG plant part is correspondingly formulated as follows:

$$\begin{cases} \dot{\mathbf{x}}_{\mathbf{plt}}(t) = \mathbf{A.plt}\cdot\mathbf{x}_{\mathbf{plt}}(t) + \mathbf{B.plt}\cdot\mathbf{u}_{\mathbf{plt}}(t) \\ \mathbf{y}_{\mathbf{plt}}(t) = \mathbf{C.plt}\cdot\mathbf{x}_{\mathbf{plt}}(t) + \mathbf{D.plt}\cdot\mathbf{u}_{\mathbf{plt}}(t) \end{cases} \tag{14}$$

$$\begin{aligned} \mathbf{x}_{plt}(t) &= \left[i_{L1}(t) \quad \cdots \quad i_{LNT}(t) \quad v_{DC}(t)\right]^T \\ \mathbf{u}_{plt}(t) &= \left[d_1(t) \quad \cdots \quad d_{NT}(t)\right]^T \\ \mathbf{y}_{plt}(t) &= \left[i_{L1}(t) \quad \cdots \quad i_{LNT}(t) \quad v_{DC}(t)\right]^T \end{aligned} \tag{15}$$

with **A.plt**, **B.plt**, **C.plt** and **D.plt** being the *state matrix*, *input matrix*, *output matrix* and *feedthrough matrix*, respectively.

B. Controller Part

The controller model is shown in Fig. 7. Four PI control loops and a droop control loop are included as described in (1)-(4). A local error e_M (%) is also considered which can be caused by transmission line parameter differences or measurement error.

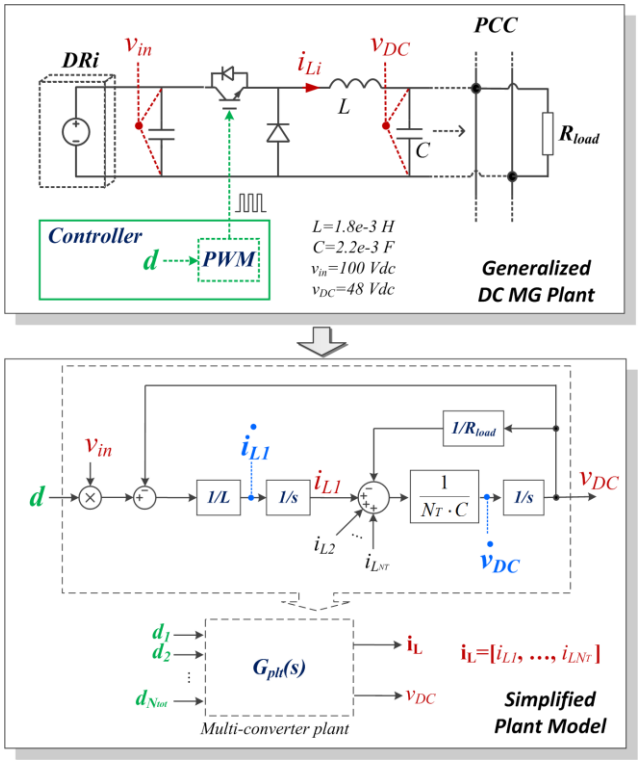

Fig. 6. DC MG plant model.

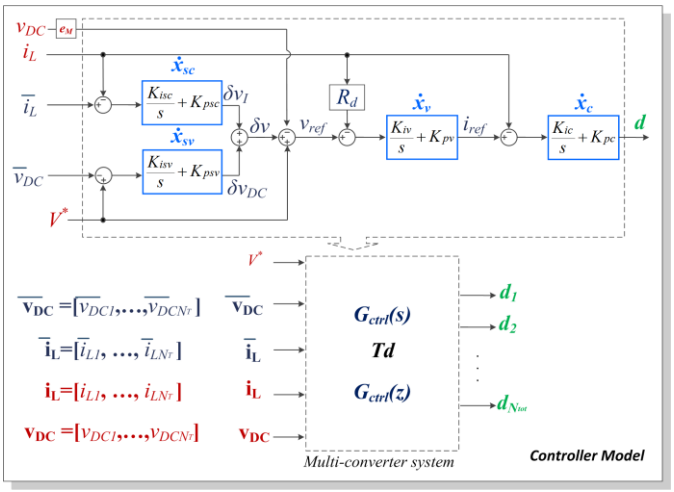

Fig. 7. Controller model.

A transfer function $G_{ctrl}(s)$ is obtained. The input variables are voltage reference (V^*), averaged measured CB voltage obtained by each local controller by using DCA ($\bar{v}_{DC1}, \ldots, v_{DCNT}$), averaged inductor current obtained by each local controller by using DCA ($i_{L1}, \ldots, i_{LNT}$), local measured CB voltage with measurement error ($v_{DC1} = v_{DC}\cdot e_{M1}, \ldots, v_{DC}\cdot e_{MNT}$) and inductor current ($i_{L1}, \ldots, i_{LNT}$). The outputs are duty ratios of the PWM signals for each converter ($d_1, \ldots, d_{NT}$). Based on the model shown in Fig. 7, the SS model of the controller part is formulated as:

$$\begin{cases} \dot{\mathbf{x}}_{\mathbf{ctrl}}(t) = \mathbf{A.ctrl}\cdot\mathbf{x}_{\mathbf{ctrl}}(t) + \mathbf{B.ctrl}\cdot\mathbf{u}_{\mathbf{ctrl}}(t) \\ \dot{\mathbf{y}}_{\mathbf{ctrl}}(t) = \mathbf{C.ctrl}\cdot\mathbf{x}_{\mathbf{ctrl}}(t) + \mathbf{D.ctrl}\cdot\mathbf{u}_{\mathbf{ctrl}}(t) \end{cases} \tag{16}$$

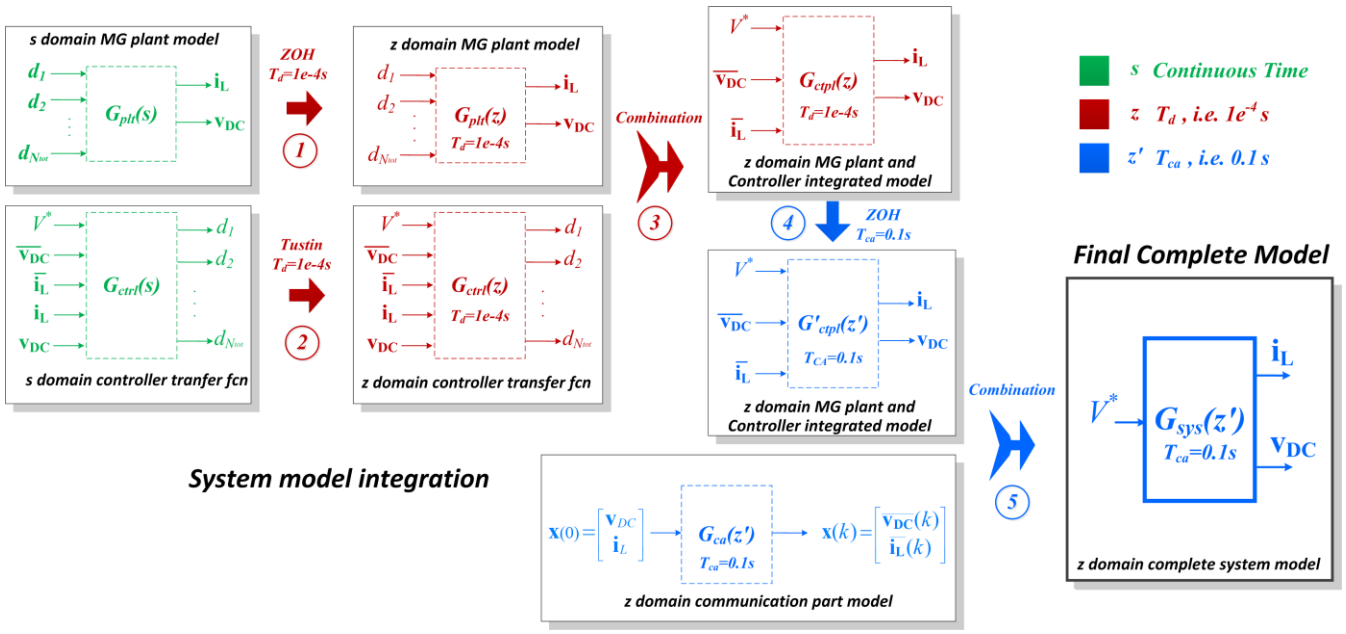

Fig. 8. System model integration.

$$
\begin{aligned}
&\mathbf{x}_{\mathbf{ctrl}}(t)=\left[\cdots \quad x_{SVi}(t) \quad x_{SCi}(t) \quad x_{Vi}(t) \quad x_{Ci}(t) \quad \cdots\right]\\
&\mathbf{u}_{\mathbf{ctrl}}(t)=\left[V^{*} \quad \bar{\mathbf{v}}_{\mathbf{DC}}(t) \quad \bar{\mathbf{i}}_{\mathbf{L}}(t) \quad \mathbf{i}_{\mathbf{L}}(t) \quad \mathbf{v}_{\mathbf{DC}}(t)\right]\\
&\bar{\mathbf{v}}_{\mathbf{DC}}(t)=\left[\bar{v}_{DC1}(t) \quad \bar{v}_{DC2}(t) \quad \cdots \quad \bar{v}_{DCNT}(t)\right]\\
&\bar{\mathbf{i}}_{\mathbf{L}}(t)=\left[\bar{i}_{L1}(t) \quad \bar{i}_{L2}(t) \quad \cdots \quad \bar{i}_{LNT}(t)\right]\\
&\mathbf{i}_{\mathbf{L}}(t)=\left[i_{L1}(t) \quad i_{L2}(t) \quad \cdots \quad i_{LNT}(t)\right]\\
&\mathbf{v}_{\mathbf{DC}}(t)=\left[v_{DC1}(t) \quad v_{DC2}(t) \quad \cdots \quad v_{DCNT}(t)\right]
\end{aligned}
\tag{17}
$$

where $\mathbf{x}_{\mathbf{ctrl}i}$ is the state vector of the i^{th} controller, as four PI controllers are included corresponding to 4 states: secondary voltage and current loop states (x_{SVi} and x_{SCi}), and inner voltage and current loop states (x_{Vi} and x_{Ci}).

Moreover, considering the facts that digital controller has fixed sampling time (T_d), the controller model needs to be discretized so as to accurately represent the control system. Since trapezoidal rule based PI controllers are used for each control loop, *Tustin approximation* [24] is applied for transferring controller model from CT form to DT form. T_d=5e^{-5}s is considered as the sampling time of the digital controller.

C. Communication Algorithm Part

The model of the communication algorithm is shown in Fig. 3. The inputs of the communication part model ($G_{ca}(z)$) are the initial states of each node ($x_i(0)$, i=1,2,…,N_T) which are locally measured voltage and current. The outputs are the states reached in each node at k^{th} iteration ($x_i(k)$). The state variables include the cumulative differences between node i and j ($\delta_{ij}(k+1)$, $j \in N_i$, N_i is the set of indexes of the agents that are connected with agent i) and the output state ($x_i(k+1)$).

Based on this scheme, and considering that the *Laplacian* matrix should also be included, (6)-(9) can be used to establish the SS model of communication part:

$$
\begin{cases}
\mathbf{x}_{\mathbf{CA}}(k+1)=\mathbf{A.ca}\cdot\mathbf{x}_{\mathbf{CA}}(k)+\mathbf{B.ca}\cdot\mathbf{u}_{\mathbf{CA}}\\
\mathbf{y}_{\mathbf{CA}}(k+1)=\mathbf{C.ca}\cdot\mathbf{x}_{\mathbf{CA}}(k)+\mathbf{D.ca}\cdot\mathbf{u}_{\mathbf{CA}}
\end{cases}
\tag{18}
$$

$$
\begin{aligned}
&\mathbf{x}_{\mathbf{CA}}(k)=\left[\boldsymbol{\delta}_{\mathbf{i,i+1}}(k) \quad \cdots \quad \boldsymbol{\delta}_{\mathbf{i,i+N_T\text{-}1}}(k) \quad \mathbf{x}_{\mathbf{i}}(k)\right]^{T}\\
&\mathbf{u}_{\mathbf{CA}}=\left[\mathbf{x}_{\mathbf{1}}(0) \quad \cdots \quad \mathbf{x}_{\mathbf{N_T}}(0)\right]^{T}\\
&\mathbf{y}_{\mathbf{CA}}(k)=\left[\mathbf{x}_{\mathbf{1}}(k) \quad \cdots \quad \mathbf{x}_{\mathbf{N_T}}(k)\right]^{T}
\end{aligned}
\tag{19}
$$

where the elements from Laplacian matrix are included in **A.ca** representing the relationship of state variables. $\boldsymbol{\delta}_{i,j}(k)$ is the cumulative difference state between node i and node j. Both the voltage and current information consensus algorithms are based on this model.

D. Model Integration

The overall system model can be obtained by integrating the three models: the plant part model in CT form (s domain), controller part model in DT form (z domain) with sampling time T_d, and communication part model in DT form with sampling time T_{ca}. The model integration requires proper handling of different sampling times and interfacing variables. The following steps are executed in order to obtain the accurate overall system model, as shown in Fig. 8: (1) The MG plant is modeled in CT form, however, the controller part measures voltage and current based on the measurement sampling time (T_d). The MG plant model is first discretized using ZOH method with the same sampling time of T_d; (2) Tustin method is used to transform the controller model from s domain to z domain with a sampling time T_d; (3) The combination of MG plant model and controller model can be realized by interfacing their input/output variables and closing loops. Duty ratios become inner states after combination; (4) In order to integrate with communication part model, the MG plant and controller combined model is discretized using ZOH method with sampling time T_{ca}; (5) Finally, the complete system model can

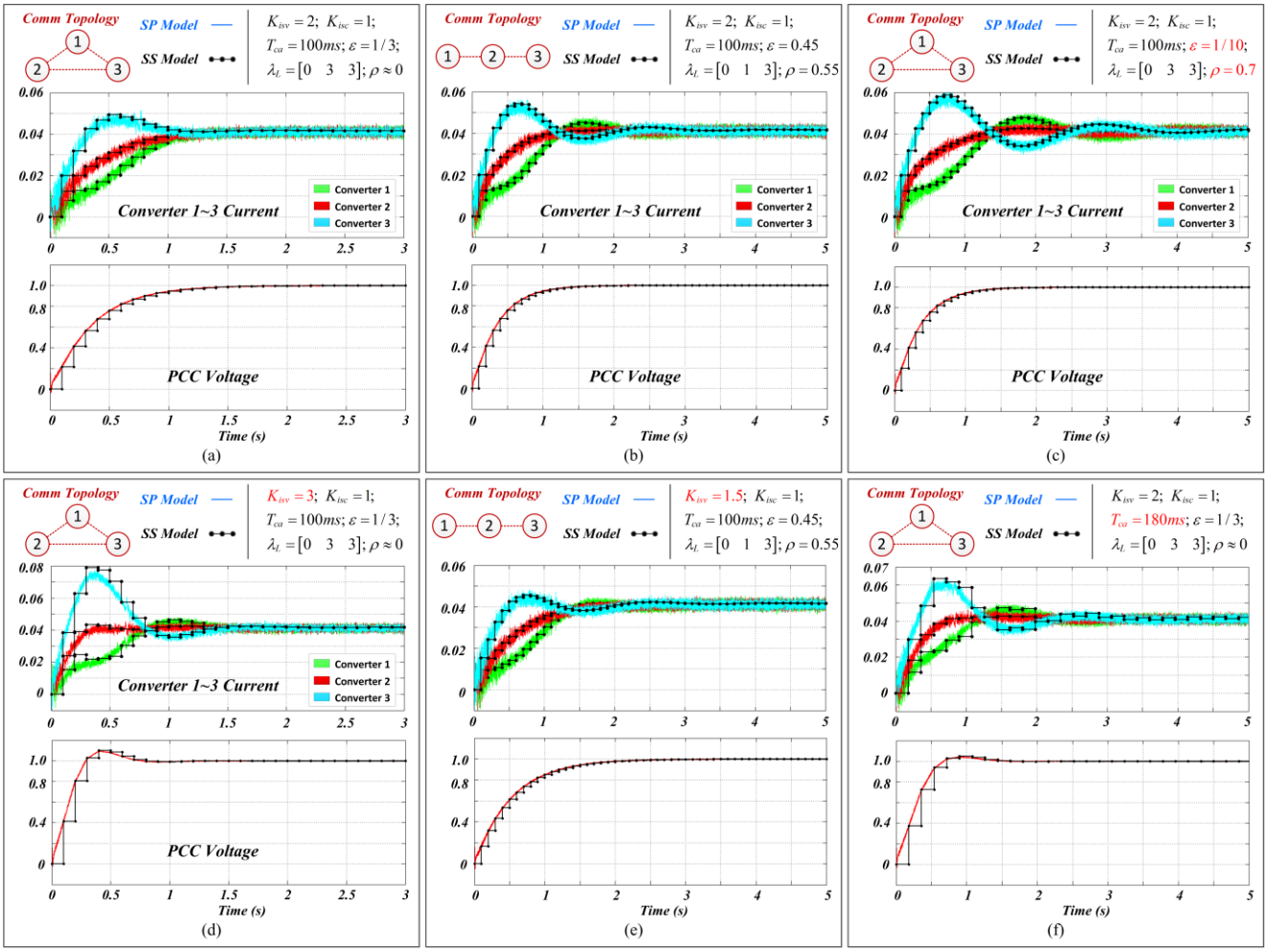

Fig. 9. 3-node system dynamics comparison: (a) with basic parameter settings shown in Table I and ring-shape communication topology; (b) with line-shape communication topology; (c) with decreased constant edge weight $\varepsilon = 1/10$; (d) with increased secondary control parameter K_{isv}=3; (e) with line-shape topology and decreased secondary control parameter K_{isv} =1.5; (f) with increased communication time step T_{ca}=180ms.

be obtained by integrating communication part model with MG plant and controller model under sampling time T_{ca}.

V. Results and Sensitivity Analysis

In order to verify the correctness of the proposed modeling approach, Simulink and PLECS are used as simulation environment. A group of paralleling buck converters is built in PLECS with the same parameters as shown in Fig. 6 (time step of $1e^{-6}$s is used to emulate the CT system). Primary and secondary control loops are implemented in Simulink with time step T_d=$5e^{-5}$s. The communication links and consensus algorithm are also formulated in Simulink with time step T_{ca} which was changed from 1ms to 1000ms. 3-unit system is simulated. The parameters of primary and secondary control loops are given in Table I. First of all, the step response of the SS model is compared with the SP model to verify the correctness of the modeling approach. Then several comparison cases are studied and discussed focusing on the system dynamics under different communication topologies, consensus algorithm parameters and control parameters. Finally, conclusions are made based on the presented results.

The step response of the SS model and SP model with different system configurations are obtained as shown in Fig. 9. Both the voltage and current are both divided by the rated voltage value (48V) so as to compare the dynamic of the SS model (dotted black curves) and SP model (colored curves). It can be seen that with different communication topologies and control parameters the step response of the SS model fits well into the SP model, which demonstrates the correctness of the modeling method. Based on this model, the system dynamics under different communication topologies, DCA adjustment steps, communication rate (time step), and control parameters are analyzed in the following part.

TABLE I. Basic Parameters of The System

Priamry Control				
Virtual Resistance	*Voltage PI Loop*		*Current PI Loop*	
R_d=0.2 Ohm	K_{pv}=4	K_{iv}=800	K_{pc}=1	K_{ic}=97
Secondary Control				
Secondary Voltage PI Loop		*Secondary Current PI Loop*		
K_{psv}=0.02	K_{isv}=2	K_{psc}=0.02	K_{isc}=1	
Emulated Measurement Error				
e_{M1}	e_{M2}		e_{M3}	
+0.8%	*+0.2%*		*-0.8%*	

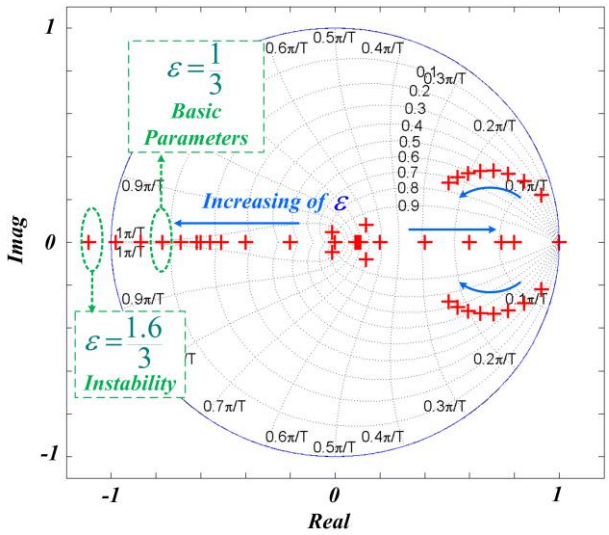

Fig. 10. Root locus analysis with ε changing from 0.2/3~1.6/3.

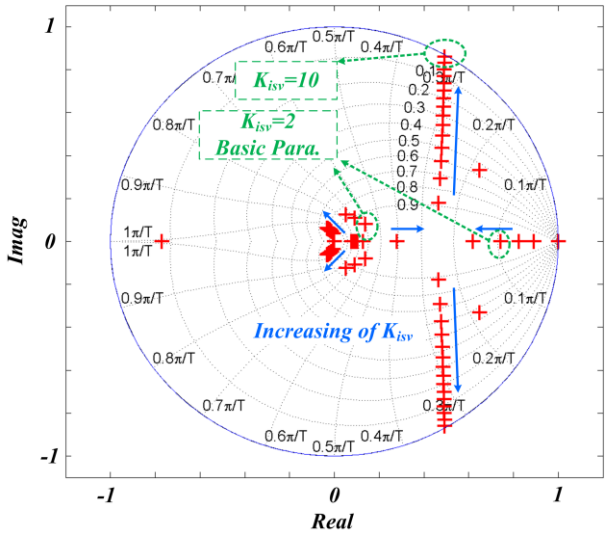

Fig. 11. Root locus analysis with K_{isv} changing from 1 to 10.

A. Topology

As can be seen from the consensus algorithm model in Fig. 3 and Eq. (8) and (9) that, the Laplacian graph of the communication topology has significant influence on the communication dynamics which consequently affects the complete system dynamics. A comparison is made between ring- and line-shape topologies as shown in Fig. 9 (a) and (b). The communication time step (T_{ca}) is considered to be 100ms. Constant edge weight ε is set to 0.45 for line-shape case and 1/3 for ring-shape case which offers the minimized spectral radius $\rho(\mathbf{W}-(1/N_T)\cdot\mathbf{1}\cdot\mathbf{1}^T)$ for both cases to ensure the fastest and stable convergence of DCA. The current and voltage curves show the dynamic of the overall system which indicates that ring-shape case offers faster and more stable response compared with line-shape case. The presented results go well in line with theory previously developed in [25] that, the algebraic connectivity and convergence speed of small world networks can be significantly improved by properly design the topology of the communication network.

B. DCA constant edge weight ε

Apart from communication topology, the constant edge weight (ε) also has decisive influence on DCA convergence, as was shown in Fig. 4. In Fig. 9 (c), under the ring-shape topology ε is changed from 1/3 to 1/10, which consequently changes $\rho(\mathbf{W}-(1/N_T)\cdot\mathbf{1}\cdot\mathbf{1}^T)$ from 0 to 0.7. The increased spectral radius indicates slower convergence speed of DCA that causes more oscillation and response transient time in Fig. 9 (c) compared with Fig. 9 (a). The root locus of the complete system model ($\boldsymbol{G}_{sys}(z)$) with ε *changing* is shown in Fig. 10. The constant edge weight ε is changed from 0.2/3~1.6/3. The basic parameter ($\varepsilon=1/3$) is chosen to keep the stable operation of the system. If the constant edge weight is set too large, the DCA appears to be oscillation (as shown in Fig. 4), which can incur system instability (see Fig. 10, $\varepsilon=1.6/3$).

C. Secondary control parameter

Compared with inner control loops, secondary control has relative lower bandwidth and slower speed. Also considering that the performance of secondary control is based on the knowledge from DCA, this control level is more interactive between nodes and should hence be designed with respect to the communication features. In Fig. 9 (d) the secondary voltage control loop parameter K_{isv} is changed as an example. It can be seen from the comparison between Fig. 9 (a) and (d) that, the increased K_{isv} results in faster response while incurs more oscillation on both voltage and current. On the contrary, in order to damping the system K_{isv} can be decreased to slower down the secondary control to match the communication speed as shown in the comparison between Fig. 9 (b) and (e). Fig. 9 (b) indicates an oscillation dynamic because of slow convergence of DCA in line-shape case, while in Fig. 9 (e) the same line-shape topology is used but K_{isv} is decreased to 1.5 offering a slower but more damped system dynamic.

The root locus of the system with K_{isv} changing is shown in Fig. 10 (b). The K_{isv} is changed from 1 to 10 under ring-shape network. It can be seen from the figure that with the increasing of K_{isv}, the system response becomes faster but occur to be more oscillating. The basic parameters keep the stable operation of the system. When K_{isv} reaches the value of 10, the system is near to be unstable.

D. Communication time step T_{ca}

Another practical issue in communication part is the communication rate which depends on the type of communication topology being used in the real system. In the study case, the communication rate is taken as the time step of the DCA (T_{ca}). The change of T_{ca} certainly has a decisive influence on the dynamics of the overall system. In Fig. 9 (f), T_{ca} is changed to 180ms simulating a slower communication case. By comparing Fig. 9 (f) with (a) we can see that, the increased T_{ca} results in longer and more oscillating convergence of the whole system. It is not hard to understand that the increasing of T_{ca} causes slower convergence of DCA and consequently affects the system dynamics. In this case it can be wise to decrease the secondary control speed so as to stabilize the system.

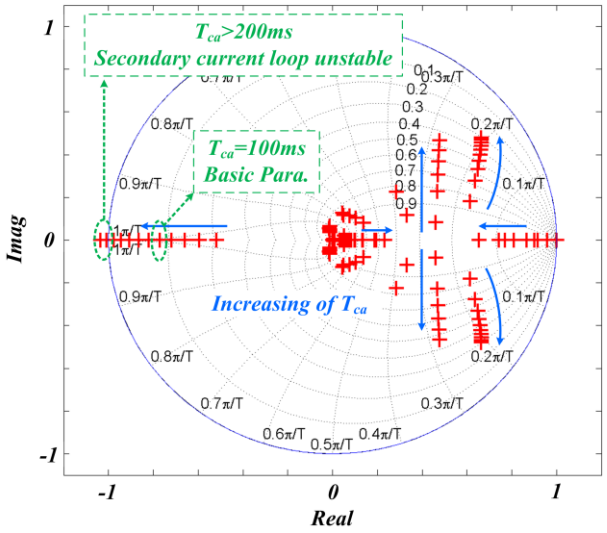

Fig. 12. Root locus analysis with T_{ca} changing from 20ms to 240ms.

The root locus with T_{ca} variations is shown in Fig. 10 (c). T_{ca} is changed from 20ms to 240ms under ring-shape network. The basic parameter case is demonstrated to be stable while with the increasing of T_{ca}, oscillations and instability might happen to the system. When T_{ca}>200ms, the system cannot keep stable operation.

VI. Conclusion

This paper investigates the modeling method for dynamic consensus algorithm based distributed hierarchical control of DC microgrids with full consideration of underlying communication topology. The hierarchical control includes inner voltage and current control loops, virtual resistance and secondary voltage and current control loops aiming at realizing accurate current sharing and keeping rated voltage amplitude in the CB. The performance of secondary control is based on the knowledge from dynamic consensus algorithm which includes the averaged voltage and current value among all the distributed resources. Accordingly, the dynamics of the system becomes more interactive. Taking into account the different sampling times of real world plant, digital controller and communication devices, the system is modeled with these three parts separately. Zero order hold and Tustin methods are used to discretize the models and integrate them into a complete system state space model. By comparing with Simulink/PLECS based model, the correctness of the state space model is justified. Finally, based on this model, the system dynamics and parameter sensitivity are studied and analyzed.

References

[1] C. Committee, D. Generation, and E. Storage, *IEEE Guide for Design , Operation , and Integration of Distributed Resource Island Systems with Electric Power Systems IEEE Standards Coordinating Committee 21 Sponsored by the*. 2011, pp. 1–54.

[2] J. M. Guerrero, J. C. Vasquez, J. Matas, L. G. De Vicuna, and M. Castilla, "Hierarchical Control of Droop-Controlled AC and DC Microgrids — A General Approach Toward Standardization," *IEEE Trans. Ind. Electron.*, vol. 58, pp. 158–172, 2011.

[3] A. Bidram and A. Davoudi, "Hierarchical Structure of Microgrids Control System," *IEEE Trans. Smart Grid*, vol. 3, pp. 1963–1976, 2012.

[4] D. E. Olivares, A. Mehrizi-Sani, A. H. Etemadi, C. A. Canizares, R. Iravani, M. Kazerani, A. H. Hajimiragha, O. Gomis-Bellmunt, M. Saeedifard, R. Palma-Behnke, G. A. Jimenez-Estevez, and N. D. Hatziargyriou, "Trends in Microgrid Control," *IEEE Trans. Smart Grid*, vol. 5, no. 4, pp. 1905–1919, Jul. 2014.

[5] M. Savaghebi, A. Jalilian, J. C. Vasquez, and J. M. Guerrero, "Secondary Control for Voltage Quality Enhancement in Microgrids," *IEEE Trans. Smart Grid*, vol. 3, no. 4, pp. 1893–1902, Dec. 2012.

[6] Q. Shafiee, C. Stefanovic, T. Dragicevic, P. Popovski, J. C. Vasquez, and J. M. Guerrero, "Robust Networked Control Scheme for Distributed Secondary Control of Islanded Microgrids," *IEEE Trans. Ind. Electron.*, vol. 61, no. 10, pp. 5363–5374, Oct. 2014.

[7] V. Nasirian, S. Moayedi, A. Davoudi, and F. Lewis, "Distributed Cooperative Control of DC Microgrids," *IEEE Trans. Power Electron.*, vol. PP, no. 99, pp. 1–1, 2014.

[8] L. Meng, T. Dragicevic, J. M. Guerrero, and J. C. Vasquez, "Optimization with system damping restoration for droop controlled DC-DC converters," in *2013 IEEE Energy Conversion Congress and Exposition*, 2013, pp. 65–72.

[9] D. E. Olivares, C. A. Canizares, and M. Kazerani, "A centralized optimal energy management system for microgrids," in *2011 IEEE Power and Energy Society General Meeting*, 2011, pp. 1–6.

[10] A. G. Tsikalakis and N. D. Hatziargyriou, "Centralized control for optimizing microgrids operation," *IEEE Trans. Energy Convers.*, vol. 23, pp. 241–248, 2008.

[11] K. T. Tan, X. Y. Peng, P. L. So, Y. C. Chu, and M. Z. Q. Chen, "Centralized Control for Parallel Operation of Distributed Generation Inverters in Microgrids," *IEEE Transactions on Smart Grid*. pp. 1–11, 2012.

[12] A. G. Tsikalakis and N. D. Hatziargyriou, "Centralized control for optimizing microgrids operation," *2011 IEEE Power Energy Soc. Gen. Meet.*, pp. 1–8, 2011.

[13] Y. Xu and W. Liu, "Novel Multiagent Based Load Restoration Algorithm for Microgrids," *IEEE Trans. Smart Grid*, vol. 2, pp. 140–149, 2011.

[14] H. Liang, B. Choi, W. Zhuang, X. Shen, A. A. Awad, and A. Abdr, "Multiagent coordination in microgrids via wireless networks," *IEEE Wireless Communications*, vol. 19. pp. 14–22, 2012.

[15] L. Meng, T. Dragicevic, J. M. Guerrero, and J. C. Vasquez, "Dynamic consensus algorithm based distributed global efficiency optimization of a droop controlled DC microgrid." pp. 1276–1283, 2014.

[16] S. Sučić, J. G. Havelka, and T. Dragičević, "A device-level service-oriented middleware platform for self-manageable DC microgrid applications utilizing semantic-enabled distributed energy resources," *Int. J. Electr. Power Energy Syst.*, vol. 54, pp. 576–588, 2014.

[17] R. Olfati-Saber and R. M. Murray, "Consensus Problems in Networks of Agents With Switching Topology and Time-Delays," *IEEE Trans. Automat. Contr.*, vol. 49, no. 9, pp. 1520–1533, Sep. 2004.

[18] R. Olfati-Saber, J. A. Fax, and R. M. Murray, "Consensus and Cooperation in Networked Multi-Agent Systems," *Proc. IEEE*, vol. 95, 2007.

[19] R. Merris, "Laplacian matrices of graphs: a survey," *Linear Algebra and its Applications*, vol. 197–198. pp. 143–176, 1994.

[20] M. Kriegleder, "A Correction to Algorithm A2 in 'Asynchronous Distributed Averaging on Communication Networks,'" vol. PP, no. 99. p. 1, 2013.

[21] N. Biggs, *Algebraic Graph Theory*, *Cambridge Tracks in Mathematics*. Cambridge, U.K.: Cambridge Univ. Press, 1974.

[22] C. Godsil and G. Royle, *Algebraic Graph Theory*, Vol. 207. New York: Springer-Verlag, 2001.

[23] L. X. L. Xiao and S. Boyd, "Fast linear iterations for distributed averaging," *42nd IEEE Int. Conf. Decis. Control (IEEE Cat. No.03CH37475)*, vol. 5, 2003.

[24] B. C. Kuo, *Digital control systems*, 2nd. oath. Forth Worth: Harcourt Brace, 1992.

[25] R. Olfati-Saber, "Ultrafast consensus in small-world networks," in *Proceedings of the 2005, American Control Conference, 2005.*, 2005, pp. 2371–2378.